ACS OMEGA

http://pubs.acs.org/journal/acsodf

Article

Role of Aryl Amphiphile Hydrophobe Size on the Concentration and Stability of Graphene Nanoplatelet Dispersions

Dorothy K. Jones, Taylor A. Watts, and Nagarjuna Gavvalapalli*

Cite This: *ACS Omega* 2021, 6, 20068−20075

Read Online

ACCESS | Metrics & More | Article Recommendations | Supporting Information

ABSTRACT: Graphene nanoplatelets (GNPs) are stable and relatively inexpensive compared to single-layer graphene sheets and carbon nanotubes and are useful in diverse electronic, optoelectronic, and mechanical applications. Solution-state processing of the active material is desired in most of the applications mentioned above, and thus, there is great interest in increasing the concentration and stability of GNP suspension. Herein, to elucidate the role of the stabilizer structural parameters on the concentration and stability of GNP dispersions, we synthesized and used a series of aryl amphiphiles (ArAs) of varying aryl hydrophobe sizes and geometries. The ArAs were found to generate GNP dispersions with concentrations ranging from 0.05 to 0.13 mg mL^{-1} depending on the size of the aryl hydrophobe. The ArAs' hydrophobe size played a key role in determining the concentration of GNP suspension, while ArAs' critical aggregation concentration and solubility limits had no impact on the GNP suspension concentration. Most of the studied ArAs work similar to methylcellulose, the previously reported best performing stabilizer . Moreover, the ArAs stabilized the GNP suspension better than methylcellulose and were able to form stable dispersions for up to 6 h. Raman studies indicate that the quality of the GNPs did not degrade during the dispersion process. These findings will aid in the development of design rules for next-generation stabilizers.

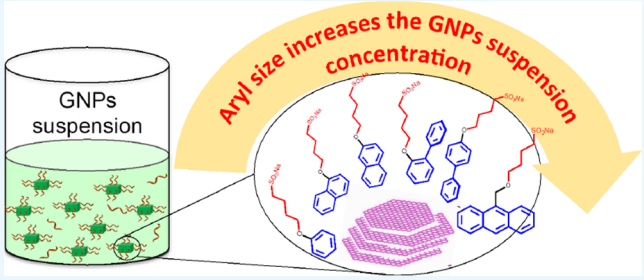

INTRODUCTION

Graphitic materials are popularly used for a wide range of applications such as in batteries,[1−6] dye-sensitized solar cells,[2,7−11] capacitors and supercapacitors,[2,12,13] and various electrochemical sensing and biosensing applications[2,14−17] due to their excellent electronic, mechanical, and optical properties, as well as their high-surface area and chemical stability.[1,2,18−22] Graphene has high Young's modulus (∼1000 GPa),[23] high intrinsic mobility (200,000 $cm^2\ v^{-1}\ s^{-1}$),[24] high thermal conductivity (5000 W $m^{-1}\ K^{-1}$),[25] large specific surface area (2630 $m^2\ g^{-1}$),[26] and excellent electrical resistivity (150 mΩ cm across the stacked sheets).[2] Of these graphitic materials, graphene nanoplatelets (GNPs) are of particular interest because they are easier to produce, have better stability than single-layer graphene,[19] and are generally cheaper than single-wall carbon nanotubes (CNTs),[27,28] and the surface of the nanoplatelets has pure graphene (sp^2 hybridized carbon) and has the same high electrical conductivity as graphene.[28] Thus, GNPs are viable substitutes for single-layer graphene and CNTs in applications such as fuel cells.[27,28] GNPs are flakes of graphite made up of a few layers of graphene in a platelet shape that generally has a diameter of 5−50 μm. For GNPs to be fully utilized for any applications, however, they need to be able to be effectively dispersed in solution.[27,28] Due to their van der Waals forces and high specific surface area, GNPs are difficult to disperse and tend to aggregate in water.[21,28−30] To combat this, GNPs and other graphitic materials are typically suspended in solution using surfactants,[31−35] polymers,[31−33] or other dispersants,[19,36,37] in combination with a physical process such as sonication.[28] Previous studies found that using poly(sodium 4-styrenesulfonate) [PSS] as a dispersant for reduced graphene oxide nanoplatelets resulted in stable dispersions of 1 mg mL^{-1}.[27] Computational calculations led to the conclusion that the edge-to-face interaction between the aryl rings of the polymer and the conjugated surface of the nanoplatelets was responsible for strong polymer binding.[27] PSS has also been used to disperse nonoxidized GNPs and resulted in more stable dispersions compared to the reference polymers that have no aryl groups (poly(diallyldimethylammonium chloride) and polyacrylic acid).[28] Wang et al.[36] have shown that methylcellulose generates the highest concentration of GNP suspension (0.1 mg mL^{-1}). To increase the concentration and stability of GNP dispersion, there is a need to understand the structural parameters and physical properties of the stabilizers that play a key role. So far, there are a handful of studies on generating GNP dispersion using

Received: June 14, 2021
Accepted: July 14, 2021
Published: July 21, 2021

https://doi.org/10.1021/acsomega.1c03126
ACS Omega 2021, 6, 20068−20075

Scheme 1. Structures of ArAs Used in This Work with Different Aryl Hydrophobes (Blue)

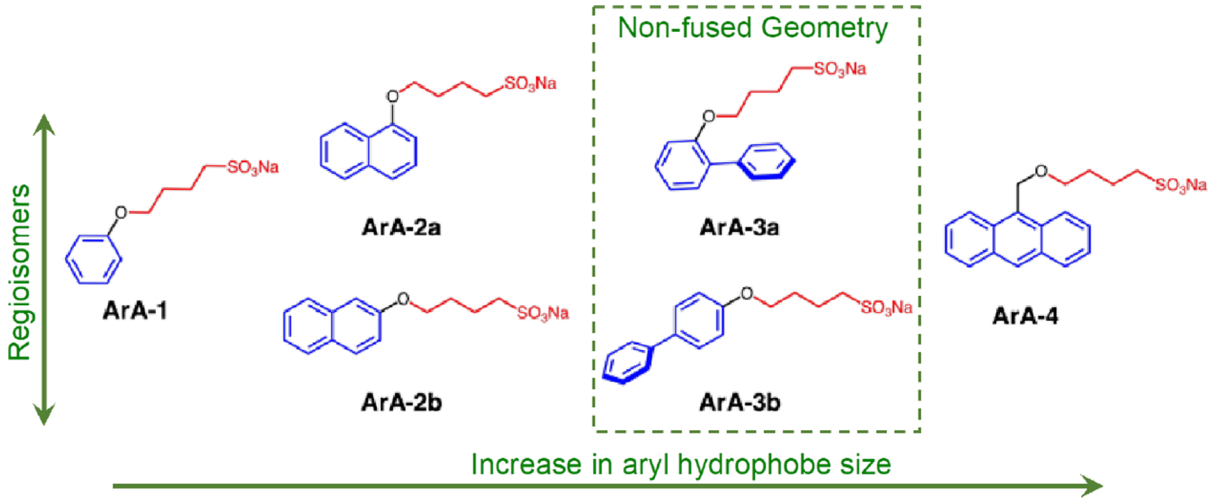

Scheme 2. Synthesis of ArAs

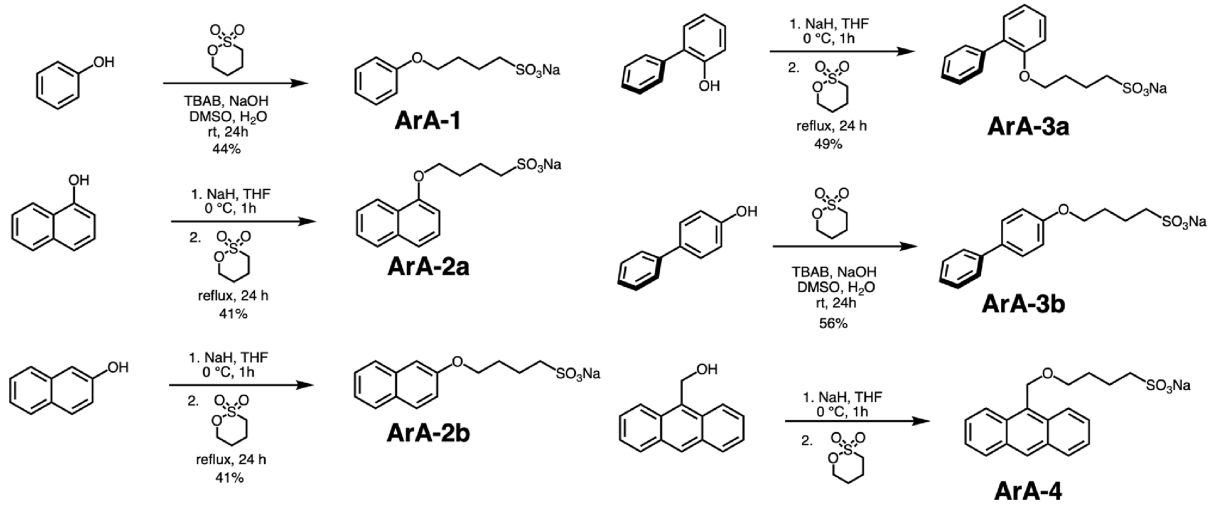

small molecule amphiphiles as well as polymer stabilizers, but there are no systematic studies.[19,29,32,36] The systematic studies will help to elucidate the role of the stabilizer structural parameters and properties in their ability to generate concentrated and stable GNP suspension.

It has been shown that amphiphiles and stabilizers containing aryl groups are more effective in generating stable and concentrated graphitic materials.[27,34,35] These aryl amphiphiles (ArAs) exhibit multiple interaction geometries with a π-face including face-to-face and edge-to-face compared to alkyl amphiphiles.[38] More importantly, ArAs exhibit higher interaction energies than the alkyl amphiphiles with a given π-face, for example, CH$-\pi$ interaction energy with a π-surface is higher for an ArA than that of an alkyl amphiphile.[39] To disperse GNPs, the amphiphile$-$GNP interaction needs to outcompete the self-association of the GNPs.[27] Therefore, in general, ArAs are more effective than alkyl amphiphiles in generating stable concentrated dispersions of graphitic materials, such as GNPs,[28,40] CNTs,[41,42] and few-layer graphene.[34,35] ArAs contain three common structural motifs: (i) an ionic headgroup, (ii) an aryl tail, and (iii) a hydrocarbon spacer between the headgroup and the aryl tail (Scheme 1). Each of these structural motifs has been shown to be useful to generate stable dispersion of graphitic materials. The ionic headgroup imparts water solubility to the ArAs. Also, the ionic head groups help to reduce aggregation of graphitic materials.[35] The aryl tail interacts with the π-face of the GNPs through $\pi-\pi$ interactions. Aryl hydrophobes interact strongly with the π-face of the graphitic material than that of alkyl surfactants, and hence, ArAs are known to stabilize the exposed π-face of the graphitic materials against aggregation.[43] The hydrocarbon spacer separates the aryl tail from the ionic headgroup, which allows the aryl tail to lay flat on the GNP surface. This face-to-face parallel configuration is difficult to achieve if the ionic group is attached directly onto the aryl group due to the repulsive interactions between the ionic group and the graphene surface.[35,44] Thus, the inclusion of the hydrocarbon spacer allows the ArAs to screen various possible interaction geometries with the GNPs and find the most stable interaction geometry. Due to the structural similarity of GNPs and other graphitic materials, we believe that the ArAs will also be effective in generating concentrated and stable dispersions of GNPs.

Recently, we have shown that ArAs are effective in stabilizing the π-face and retarding the growth of π-conjugated microcrystals along the π-stacking direction compared to alkyl

https://doi.org/10.1021/acsomega.1c03126
ACS Omega 2021, 6, 20068−20075

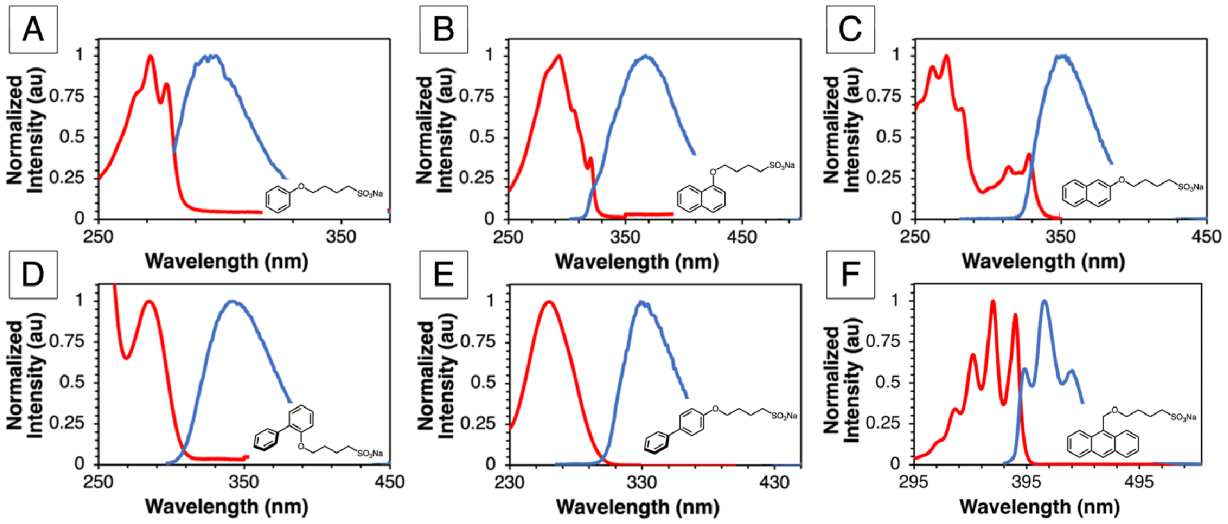

Figure 1. UV−vis absorption (red color line) and fluorescence emission spectra (blue color line) of (A) ArA-1, (B) ArA-2a, (C) ArA-2b, (D) ArA-3a, (E) ArA-3b, and (F) ArA-4.

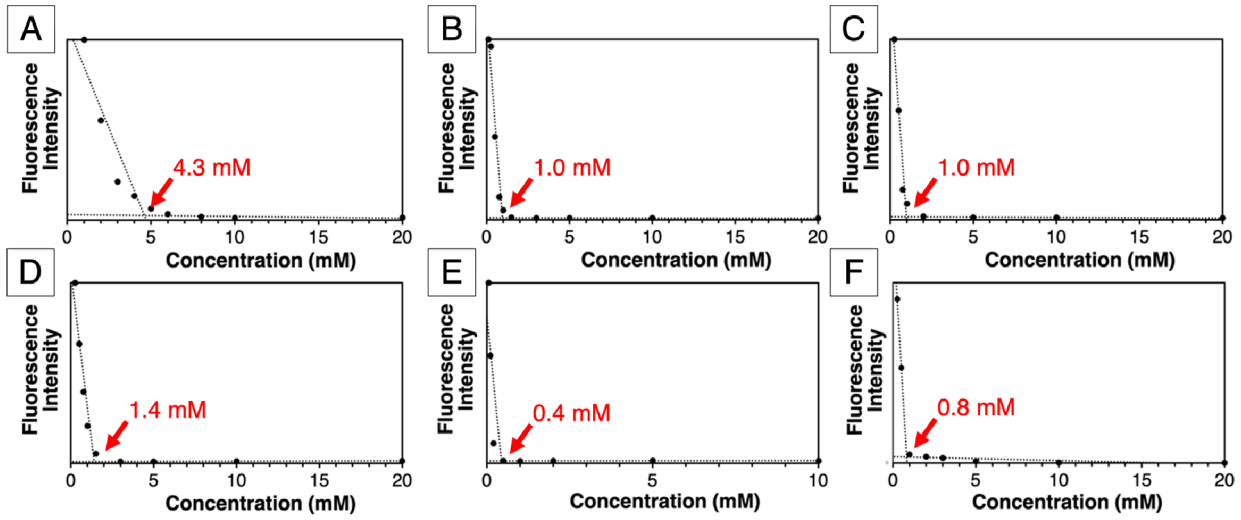

Figure 2. Concentration vs fluorescence intensity plots recorded in water for (A) ArA-1 (λ_{ex} = 271 nm), (B) ArA-2a (λ_{ex} = 293 nm), (C) ArA-2b (λ_{ex} = 271 nm), (D) ArA-3a (λ_{ex} = 287 nm), (E) ArA-3b (λ_{ex} = 255 nm), and (F) ArA-4 (λ_{ex} = 376 nm).

amphiphiles.[38,45,46] Moreover, the relative growth rate of the π-stacking facet compared to other facets is varied by changing the size of the ArA hydrophobe. Since generating stable and concentrated GNP dispersion also depends on the π-face interaction strength of stabilizer−GNP, we propose that the size of the ArA hydrophobe acts as a knob to tune the interaction strength with GNPs and provides control over the dispersion concentration. Thus, by systematically using a series of ArAs of increasing hydrophobe size, the role of the hydrophobe size in the concentration and stability of GNP dispersion can be studied.

To this end, in this work, a series of ArAs (Scheme 1) were designed and synthesized to investigate which structural parameters and physical properties of amphiphiles impact GNP dispersion. We investigated whether the critical aggregation concentration (CAC) or solubility limits were correlated with the size of the aryl hydrophobe. Both these physical properties of ArAs (solubility limit and CAC) have no effect on GNP dispersion and stability. ArA ability to generate GNP dispersion depends on the hydrophobe size. All of the ArAs with the exception of ArA-1 work similar to methylcellulose, previously reported best performing stabilizer, and result in a GNP suspension of concentration ca. 0.1 mg mL^{-1}. Moreover, ArAs stabilize the GNP suspension better than methylcellulose.

RESULTS AND DISCUSSION

Physical Characterization. The six ArAs were designed not only to have the three key structural motifs discussed above but also to represent a range of aryl sizes, geometries, and isomeric structures (Scheme 1). The sizes range from a single aromatic benzene ring (6 carbons) to naphthalene (10 carbons), biphenyl (12 carbons), and anthracene (14 carbons). The geometries vary from planar naphthyl and anthryl to twisted biphenyl structures. The two structural isomers of both substituted naphthyl and substituted biphenyl were synthesized. The ArAs were synthesized as shown in Scheme 2.

The UV−vis absorbance and emission spectra of the ArAs in water were recorded and are shown in Figure 1. The molar extinction coefficient of ArAs is also determined (Figures S1−

https://doi.org/10.1021/acsomega.1c03126
ACS Omega 2021, 6, 20068−20075

Table 1. Solubility Limit and CAC of ArAs in Water

	ArA-1	ArA-2a	ArA-2b	ArA-3a	ArA-3b	ArA-4
molecular weight (g mol^{-1})	252	302	302	328	328	366
max. solubility (mM)	38 ± 13	70 ± 3	48 ± 4	71 ± 0.5	7.5 ± 0.4	112 ± 26
CAC (mM)	4.3	1.0	1.0	1.4	0.4	0.8

Table 2. Physical Properties of GNPs

product	particle diameter (μm)	thickness (nm)	density (g/cc)	purity (%)	thermal conductivity (W/m K)	electrical conductivity (S/m)	tensile modulus (GPa)	tensile strength (GPa)
Strem 06-0215	15	6−8	0.03−0.1	>99.5	3000	10^7	1000	5

S6, Table S1), to calculate the solubility limits of the ArAs. While there are a handful of reports on the use of ArAs for a wide range of applications, the systematic studies on ArA physical properties such as their solubility or their tendency to aggregate are scarce. Knowledge of the solubility and CAC of the ArAs allows for the examination of any correlations between these properties and the effectiveness of the ArAs for different applications including generating stable GNP dispersions. The CAC of the ArAs in water was studied using concentration-dependent fluorescence experiments. The emission intensity of ArAs decreased with the increase in the concentration, as shown in Figures S7−S12, indicating aggregation-induced emission quenching in solution. The CAC of the ArAs was determined by plotting the concentration versus the emission intensity and finding the intersection of the high intensity and low intensity trendlines (Figure 2 and Table 1). The CAC of an amphiphile is inversely correlated with the size and thus the hydrophobicity of its hydrophobic group.[47] This trend is observed in the phenyl-, naphthyl-, and anthryl-based ArAs (ArA-1, 2a, 2b, and 4, respectively). ArA-2a and 2b, naphthyl-based regioisomers, have the same CAC. Unlike the naphthyl isomers, the biphenyl isomers (ArA-3a and 3b) have different CACs (1.4 and 0.4 mM, respectively). The interphenyl dihedral angle in ArA-3a is higher than that in ArA-3b due to the substitution at the second position. The higher twist between the phenyls in ArA-3a hampers ArA aggregation, resulting in higher CAC than the ArA-3b. On the other hand, ArA-3b has the larger spatial separation of the ionic head group from the phenyl substituent, which allows it to aggregate at a lower concentration than the ArA-3a (structural isomer) and ArA-4 (has more number of carbons than the biphenyl unit). This indicates that in addition to the size, both the geometry and the position of the aryl hydrophobe relative to the hydrocarbon spacer also have an impact on the CAC.

The maximum solubility of the ArAs in water (Table 1) was determined by dissolving each ArA in water at elevated temperature and then slowly cooling the solution. The resulting solution was syringe filtered and diluted, and the concentration was determined using UV−vis spectroscopy and Beer−Lambert's law. Interestingly, the solubility limit trend does not correlate well with the size of the hydrophobe. ArA-3b has the lowest solubility limit (7.5 ± 0.4 mM), and ArA-4 has the highest solubility limit (112 ± 26 mM). The lowest solubility limit of ArA-3b is due to the extended aryl architecture, which keeps the ionic tail far away from the phenyl substituent and allows the aggregation of the aryl hydrophobe better than the other ArAs. Interestingly, ArA-1 with the smallest hydrophobe has the second lowest solubility limit and ArA-4 with the largest hydrophobe has the highest solubility limit. A change in the aryl hydrophobe structure varies the ArA's critical packing parameter and hence the aggregate structure as well as the energy of crystallization of the amphiphiles. Both these factors affect the concentration at which the amphiphiles transition from aggregates in solution to hydrated crystals. Detailed studies focusing on the temperature- and concentration-dependent aggregation behavior of ArAs including the aggregate structure and number will shed light on the structural parameters that determine the solubility limits of ArAs. These studies are beyond the scope of this work.

Suspension of GNPs. GNPs (15 μm width, 6−8 nm thickness) used in this study were purchased from Strem Chemicals. The physical properties of the GNPs used in this study are summarized in Table 2. GNP suspensions were prepared by adding 5 mL of 10 mM aqueous ArA solution (with the exception of ArA-3b where a concentration of 7.5 mM was used due to the lower solubility) to 20 mg of GNPs. The solutions were sonicated in a sonic bath for 60 min. The mixtures were then centrifuged at 3000 rpm for 60 min. The supernatant was collected, and the concentration of GNPs in the solution was determined via UV−vis spectroscopy (Figures S13−S15). The optical density at 660 nm and a molar extinction coefficient of 1506 mL mg^{-1} m^{-1} were used to calculate the concentration using Beer−Lambert's law[34,37,48] The results for the dispersion experiments are summarized in Figure 3. The size of the aryl hydrophobe seemed to be the main factor that affected the GNP dispersion, with the smallest amphiphile (ArA-1) producing a GNP concentration of 0.05 ± 0.004 mg mL^{-1} and the largest amphiphile (ArA-4) producing 0.13 ± 0.001 mg mL^{-1}. The four amphiphiles in the middle of

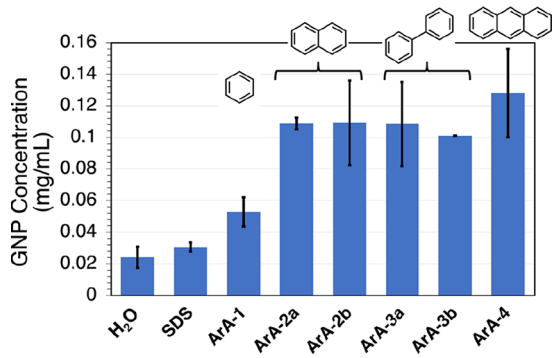

Figure 3. ArA-dependent GNP suspension concentration. The error bars represent the standard deviation calculated from three measurements.

https://doi.org/10.1021/acsomega.1c03126
ACS Omega 2021, 6, 20068−20075

the size series (ArA-2a/b and 3a/b) all produced a very similar amount of GNPs (0.10−0.11 mg mL^{-1}). Of the three structural factors (size, geometry, and isomeric structure) that were screened, the aryl size of the amphiphiles seemed to be the only factor that had any effect on the GNP dispersion efficiency. Any difference between the isomeric forms, either ArA-2a/b or ArA-3a/b, was negligible and within the margin of error. The twisted shape of the biphenyl amphiphiles (ArA-3a and 3b) seemed to have no effect compared to the planar naphthyl amphiphiles.

Overall, the use of each of these ArAs yielded a GNP dispersion with the concentration around 0.1 mg mL^{-1}, which is a much larger concentration of dispersed GNPs compared to the aliphatic control molecule [sodium dodecyl sulfate (SDS), 0.03 ± 0.003 mg mL^{-1}] and the control solution of pure water (0.02 ± 0.007 mg mL^{-1}). There have been very few examples in the literature that characterize the concentration of dispersed GNPs in aqueous solutions, but all of the reported examples were only able to disperse GNPs up to a maximum concentration of 0.1 mg mL^{-1}, which was achieved using methylcellulose as a dispersant at a concentration of 0.7 mg mL^{-1}.[29,36] It is gratifying to report that all of the studied ArAs perform as good as methylcellulose with the exception of ArA-1.

To determine the optimal amphiphile concentration for the GNP dispersion, a range of amphiphile concentrations were tested using ArA-2a as a model amphiphile. The same dispersion procedure described above was used except that the ArA-2a concentration was varied from 2 to 60 mM. The GNP dispersion efficiency was higher when the amphiphile concentration was between 5 and 20 mM and was lower below and above this concentration regime (Figures 4 and S16).

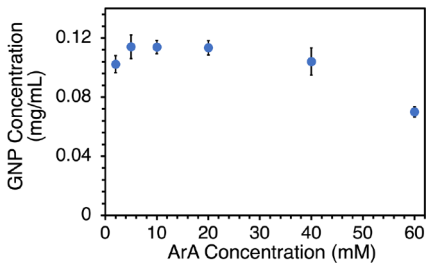

Figure 4. Concentration of GNPs dispersed with different ArA concentrations.

Of the few studies that have been performed on GNP dispersion in aqueous solutions,[19,29,32,36] none has investigated the physical properties that affect the dispersion efficacy of amphiphiles. It has been hypothesized that the solubility of an amphiphile in water influences its dispersion efficiency,[34] but there are no studies done to test this. Herein, we show that at least for the series of ArAs tested, there is no correlation between the CAC, solubility limits of ArAs, and the GNP dispersion. Each of the isomeric pairs (ArA-2a/b and ArA-3a/b) were found to have similar abilities to disperse GNPs, despite the differences in their solubility limits. For the series of amphiphiles studied here, the size of the aryl hydrophobe is the only key factor in determining the concentration of GNP dispersion. An aryl hydrophobe containing 10 or more carbons yielded GNP suspensions of almost similar concentration, indicating that there is not much gain in the GNP suspension concentration beyond this size.[19]

Stability and Quality of GNP Suspensions. While dispersing a high concentration of GNPs in solution is an important step, the generated dispersions should be stable against aggregation for their use in different applications. For this study, ArA-2a was once again used as a model amphiphile. The stability of the GNP suspensions was determined by measuring the transmittance of the solutions at different time intervals over 24 h, where a lower transmittance indicates a more stable dispersion (Figures 5A,B). The GNP suspension that was dispersed using ArA-2a showed only a slight increase in the transmittance, indicating that the dispersions are relatively stable. The initial transmittances of GNP dispersion in ArA-2 and methylcellulose[36] are 18% and 35%, which dropped to 35% and 62% after 24 h, respectively. The low transmittance value at the start as well as only a small raise even after 24 h indicates that ArA-2 is a better stabilizer for GNP suspension than methylcellulose. In contrast, the stability of the control GNP suspension without any surfactant or amphiphile decreases rapidly over the whole 24 h period (Figure S17). The ArAs impart better time-dependent stability against aggregation to GNP dispersions compared to both previously reported stabilizers and the control sample without any stabilizers.

Maintaining the quality of the GNPs, i.e., the integrity of the chemical structure during the dispersion process, is critical for electronic and optoelectronic applications. Given the long sonication time, it would not be unusual for the GNPs to show some degradation. Indeed, in previously reported examples of GNP dispersions the quality of the GNPs usually decreases after suspension, with defects forming and more oxygen-containing groups being introduced.[29,32] Raman spectroscopy is commonly used to characterize the quality and/or degradation of graphitic materials including GNPs.[29,30] The

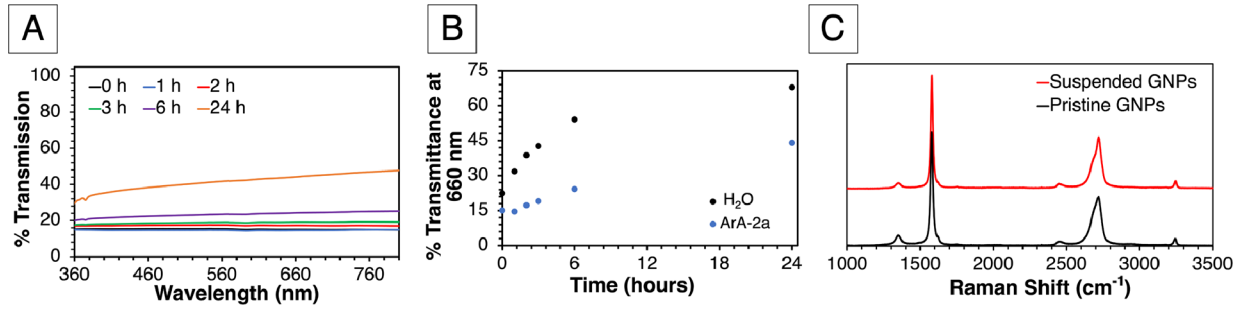

Figure 5. (A) Time-dependent change in %transmittance of GNPs suspended in ArA-2a, (B) %transmittance at 660 nm of GNPs suspended in H_2O and ArA-2a solution at different time intervals, and (C) Raman spectra of GNPs after suspension in ArA-2a and pristine GNPs.

https://doi.org/10.1021/acsomega.1c03126
ACS Omega 2021, 6, 20068−20075

three main graphitic Raman peaks are the G-peak at 1580 cm^{-1}, the D-peak at 1350 cm^{-1}, and the 2D peak at 2690 cm^{-1}, with the D-peak being related to sp^3 vibrations and to the presence of defects in the lattice.[29,30] The GNPs that had been suspended in ArA-2a were spin-coated onto a silicon wafer, and their Raman spectrum was recorded for comparison with a pristine GNP Raman spectrum (Figure 5C). The lack of peak broadening and lack of change in the D-peak intensity between the pristine GNP and dispersed GNP spectra confirm that the GNPs do not degrade after sonication with the ArAs. It has been shown that in few cases, the dispersion of GNPs resulted in the destruction of the regular structure of the GNPs,[21,29] which limits the potential use of the GNPs in optoelectronic applications. The ArAs used in this study, fortunately, resulted in pristine GNPs after dispersion. Thus, the ArAs are a more viable option for the dispersion of GNPs for such applications.

CONCLUSIONS

To understand the key structural parameters that play a key role in generating concentrated and stable GNP dispersion, a series of ArAs of varying aryl group sizes and geometries are synthesized and studied. The ArA CAC increases with the size of the aryl hydrophobe, while the solubility limit shows no trend. Also, surprisingly CAC and solubility limit of the ArAs have no effect on the GNP suspension concentration. The size of the ArA hydrophobe is the only key parameter that determines the GNP suspension concentration. Within the series, there is not much gain in the GNP suspension concentration beyond 10 carbons in the aryl hydrophobe. Also, the geometry and regioisomerism of the aryl hydrophobes have no impact on the dispersion concentration. All of the ArAs (except ArA-1) studied here work similar to the previously reported best performing stabilizer (methylcellulose). The ArAs stabilize the GNP suspension better than methylcellulose. Therefore, ArAs are a good class of stabilizers for generating GNP dispersions. Thus, future studies should focus on the impact of ArAs on other structural parameters including the electronic nature of the aryl hydrophobe, hydrocarbon spacer, and hydrophilic group on the GNP dispersion.

EXPERIMENTAL SECTION

Reagents for synthesis were purchased from Alfa Aesar, Fisher, Frontier Scientific, Acros, and Sigma-Aldrich and used as received. GNPs were purchased from Strem Chemicals. HPLC grade water was purchased from Fisher.

ArA-1, 2b, 3b, and 4 were synthesized according to the previously reported protocols from our group,[38,45,46] while ArA-2a and 3a were newly synthesized from the corresponding alcohol through the nucleophilic addition of 1,4-butane sultone (Scheme 2 and see the Supporting Information for full synthetic details). The resulting ArAs were purified via reverse phase chromatography, with the exception of ArA-3b, which was purified via recrystallization in water and dimethyl sulfoxide.

UV−vis absorbance spectra of the ArAs were recorded on an Agilent Technologies Cary Series 5000 UV−vis−NIR spectrophotometer. Fluorescence emission spectra were recorded on a Horiba Scientific FluoroMax-4 spectrofluorometer. The Raman data was collected using a Horiba Instruments LabRAM HR evolution confocal Raman microscope. The suspended GNP solutions were spin-coated onto a silicon wafer, and the data was obtained through a 100 magnification lens, using a 532 nm laser. The Raman scattering signals were collected using an 1800 lines/mm grating, at a laser power of 100%.

ASSOCIATED CONTENT

Supporting Information

The Supporting Information is available free of charge at https://pubs.acs.org/doi/10.1021/acsomega.1c03126.

ArA synthesis details and NMR spectra, Beer's law plots, concentration-dependent fluorescence spectra, UV−vis spectra of GNP dispersions, time-dependent GNP dispersion stability, and photograph of GNP dispersions (PDF)

AUTHOR INFORMATION

Corresponding Author

Nagarjuna Gavvalapalli − *Department of Chemistry and Institute for Soft Matter Synthesis and Metrology, Georgetown University, Washington, D.C. 20057, United States*; orcid.org/0000-0002-2812-1694; Email: ng554@georgetown.edu

Authors

Dorothy K. Jones − *Department of Chemistry and Institute for Soft Matter Synthesis and Metrology, Georgetown University, Washington, D.C. 20057, United States*

Taylor A. Watts − *Department of Chemistry, Georgetown University, Washington, D.C. 20057, United States*

Complete contact information is available at: https://pubs.acs.org/10.1021/acsomega.1c03126

Notes

The authors declare no competing financial interest.

ACKNOWLEDGMENTS

We thank the Donors of the American Chemical Society Petroleum Research Fund (#58444-DNI7), the National Science Foundation CAREER Grant (NSF-1944184), and the Georgetown University start-up funds for partial support of this research. D.K.J. thanks the Clare Boothe Luce Foundation.

REFERENCES

(1) Zhai, Y.; Dou, Y.; Zhao, D.; Fulvio, P. F.; Mayes, R. T.; Dai, S. Carbon materials for chemical capacitive energy storage. *Adv. Mater.* **2011**, *23*, 4828−4850.

(2) Ambrosi, A.; Chua, C. K.; Bonanni, A.; Pumera, M. Electrochemistry of graphene and related materials. *Chem. Rev.* **2014**, *114*, 7150−7188.

(3) Geim, A. K.; Novoselov, K. S. The rise of graphene. *Nat. Mater.* **2007**, *6*, 183−191.

(4) Han, S.; Wu, D.; Li, S.; Zhang, F.; Feng, X. Graphene: A two-dimensional platform for lithium storage. *Small* **2013**, *9*, 1173−1187.

(5) Dahn, J. R.; Zheng, T.; Liu, Y.; Xue, J. S. Mechanisms for Lithium Insertion in Carbonaceous Materials. *Science* **1995**, *270*, 590−593.

(6) Pan, D.; Wang, S.; Zhao, B.; Wu, M.; Zhang, H.; Wang, Y.; Jiao, Z. Li Storage Properties of Disordered Graphene Nanosheets. *Chem. Mater.* **2009**, *21*, 3136−3142.

(7) Kavan, L.; Yum, J. H.; Nazeeruddin, M. K.; Gratzel, M. Graphene Nanoplatelet Cathode for Co(III)/(II) Mediated Dye-Sensitized Solar Cells. *ACS Nano* **2011**, *5*, 9171−9178.

(8) Kavan, L.; Yum, J. H.; Gratzel, M. Graphene nanoplatelets outperforming platinum as the electrocatalyst in co-bipyridine-mediated dye-sensitized solar cells. *Nano Lett.* **2011**, *11*, 5501−5506.
(9) Kavan, L.; Yum, J. H.; Gratzel, M. Optically Transparent Cathode for Dye-Sensitized Solar Cells Based on Graphene Nanoplatelets. *ACS Nano* **2011**, *5*, 165−172.
(10) Grätzel, M. Dye-sensitized solar cells. *J. Photochem. Photobiol., C* **2003**, *4*, 145−153.
(11) Kavan, L.; Yum, J.-H.; Graetzel, M. Application of graphene-based nanostructures in dye-sensitized solar cells. *Phys. Status Solidi B* **2013**, *250*, 2643−2648.
(12) Pumera, M. Graphene-based nanomaterials for energy storage. *Energy Environ. Sci.* **2011**, *4*, 668−674.
(13) Kim, T.; Lim, S.; Kwon, K.; Hong, S.-H.; Qiao, W.; Rhee, C. K.; Yoon, S.-H.; Mochida, I. Electrochemical Capacitances of Well-Defined Carbon Surfaces. *Langmuir* **2006**, *22*, 9086−9088.
(14) Qiu, J.-D.; Huang, J.; Liang, R.-P. Nanocomposite film based on graphene oxide for high performance flexible glucose biosensor. *Sens. Actuators, B* **2011**, *160*, 287−294.
(15) Kang, X.; Wang, J.; Wu, H.; Aksay, I. A.; Liu, J.; Lin, Y. Glucose oxidase-graphene-chitosan modified electrode for direct electrochemistry and glucose sensing. *Biosens. Bioelectron.* **2009**, *25*, 901−905.
(16) Goh, M. S.; Bonanni, A.; Ambrosi, A.; Sofer, Z.; Pumera, M. Chemically-modified graphenes for oxidation of DNA bases: Analytical parameters. *Analyst* **2011**, *136*, 4738−4744.
(17) Goh, M. S.; Pumera, M. Number of graphene layers exhibiting an influence on oxidation of DNA bases: Analytical parameters. *Anal. Chim. Acta* **2012**, *711*, 29−31.
(18) Han, J.; Zhang, L. L.; Lee, S.; Oh, J.; Lee, K.-S.; Potts, J. R.; Ji, J.; Zhao, X.; Ruoff, R. S.; Park, S. Generation of B-Doped Graphene Nanoplatelets Using a Solution Process and Their Supercapacitor Applications. *ACS Nano* **2013**, *7*, 19−26.
(19) Poon, J.; Batchelor-Mcauley, C.; Tschulik, K.; Compton, R. G. Single graphene nanoplatelets: Capacitance, potential of zero charge and diffusion coefficient. *Chem. Sci.* **2015**, *6*, 2869−2876.
(20) Castro Neto, A. H.; Guinea, F.; Peres, N. M. R.; Novoselov, K. S.; Geim, A. K. The electronic properties of graphene. *Rev. Mod. Phys.* **2009**, *81*, 109−162.
(21) Wang, L.; Xin, B.; Elsukova, A.; Eklund, P.; Solin, N. Mechanochemical Formation of Protein Nanofibril: Graphene Nanoplatelet Hybrids and Their Thermoelectric Properties. *ACS Sustainable Chem. Eng.* **2020**, *8*, 17368−17378.
(22) Luo, Q.; Wirth, C.; Pentzer, E. Efficient sizing of single layer graphene oxide with optical microscopy under ambient conditions. *Carbon* **2020**, *157*, 395−401.
(23) Lee, C.; Wei, X.; Kysar, J. W.; Hone, J. Measurement of the Elastic Properties and Intrinsic Strength of Monolayer Graphene. *Science* **2008**, *321*, 385−388.
(24) Bolotin, K. I.; Sikes, K. J.; Jiang, Z.; Klima, M.; Fudenberg, G.; Hone, J.; Kim, P.; Stormer, H. L. Ultrahigh electron mobility in suspended graphene. *Solid State Commun.* **2008**, *146*, 351−355.
(25) Balandin, A. A.; Ghosh, S.; Bao, W.; Calizo, I.; Teweldebrhan, D.; Miao, F.; Lau, C. N. Superior Thermal Conductivity of Single-Layer Graphene. *Nano Lett.* **2008**, *8*, 902−907.
(26) Zhu, Y.; Murali, S.; Cai, W.; Li, X.; Suk, J. W.; Potts, J. R.; Ruoff, R. S. Graphene and graphene oxide: Synthesis, properties, and applications. *Adv. Mater.* **2010**, *22*, 3906−3924.
(27) Stankovich, S.; Piner, R. D.; Chen, X.; Wu, N.; Nguyen, S. T.; Ruoff, R. S. Stable aqueous dispersions of graphitic nanoplatelets via the reduction of exfoliated graphite oxide in the presence of poly(sodium 4-styrenesulfonate). *J. Mater. Chem.* **2006**, *16*, 155−158.
(28) Lu, J.; Do, I.; Fukushima, H.; Lee, I.; Drzal, L. T. Stable Aqueous Suspension and Self-Assembly of Graphite Nanoplatelets Coated with Various Polyelectrolytes. *J. Nanomater.* **2010**, *2010*, 1−11.
(29) Wang, B.; Liang, X. Surface Decoration and Dispersibility of Graphene Nanoplatelets in Aqueous Surfactant Solution. *J. Nanosci. Nanotechnol.* **2019**, *19*, 2060−2069.
(30) Ding, J. H.; Zhao, H. R.; Yu, H. B. A water-based green approach to large-scale production of aqueous compatible graphene nanoplatelets. *Sci. Rep.* **2018**, *8*, No. 5567.
(31) Moore, V. C.; Strano, M. S.; Haroz, E. H.; Hauge, R. H.; Smalley, R. E. Individually suspended single-walled carbon nanotubes in various surfactants. *ACS Nano* **2003**, *3*, 1379−1382.
(32) Wang, B.; Deng, S.; Zhao, L. Modification of Ultraviolet Spectrophotometry Representational Method in Graphene Nanoplates Dispersion. *J. Nanosci. Nanotechnol.* **2020**, *20*, 4015−4022.
(33) Guardia, L.; Fernández-Merino, M. J.; Paredes, J. I.; Solís-Fernández, P.; Villar-Rodil, S.; Martínez-Alonso, A.; Tascón, J. M. D. High-throughput production of pristine graphene in an aqueous dispersion assisted by non-ionic surfactants. *Carbon* **2011**, *49*, 1653−1662.
(34) Zhang, L.; Zhang, Z.; He, C.; Dai, L.; Liu, J.; Wang, L. Rationally Designed Surfactants for Few-Layered Graphene Exfoliation: Ionic Groups Attached to Electron-Deficient π-Conjugated Unit through Alkyl Spacers. *ACS Nano* **2014**, *8*, 6663−6670.
(35) Heard, K. W. J.; Bartlam, C.; Williams, C. D.; Zhang, J.; Alwattar, A. A.; Little, M. S.; Parry, A. V. S.; Porter, F. M.; Vincent, M. A.; Hillier, I. H.; Siperstein, F. R.; Vijayaraghavan, A.; Yeates, S. G.; Quayle, P. Initial Studies Directed toward the Rational Design of Aqueous Graphene Dispersants. *ACS Omega* **2019**, *4*, 1969−1981.
(36) Wang, B.; Jiang, R.; Song, W.; Liu, H. Controlling dispersion of graphene nanoplatelets in aqueous solution by ultrasonic technique. *Russ. J. Phys. Chem. A* **2017**, *91*, 1517−1526.
(37) Ruse, E.; Larboni, M.; Lavi, A.; Pyrikov, M.; Leibovitch, Y.; Ohayon-Lavi, A.; Vradman, L.; Regev, O. Molten salt in-situ exfoliation of graphite to graphene nanoplatelets applied for energy storage. *Carbon* **2021**, *176*, 168−177.
(38) Jones, D. K.; Kerwin, B.; Zhao, W.; Gavvalapalli, N. Aryl amphiphile shape-directors for shape-controlled synthesis of organic semiconductor particles. *Chem. Commun.* **2019**, *55*, 1306−1309.
(39) Ribas, J.; Cubero, E.; Luque, F. J.; Orozco, M. Theoretical Study of Alkyl-π and Aryl-π Interactions. Reconciling Theory and Experiment. *J. Org. Chem.* **2002**, *67*, 7057−7065.
(40) Mohamed, A.; Ardyani, T.; Abu Bakar, S.; Sagisaka, M.; Umetsu, Y.; Hamon, J. J.; Rahim, B. A.; Esa, S. R.; Abdul Khalil, H. P. S.; Mamat, M. H.; King, S.; Eastoe, J. Rational design of aromatic surfactants for graphene/natural rubber latex nanocomposites with enhanced electrical conductivity. *J. Colloid Interface Sci.* **2018**, *516*, 34−47.
(41) Welsh, D. J.; O'Driscoll, L. J.; Bailey, S. W. D.; Visontai, D.; Howes, K.; Frampton, H.; Bryce, M. R.; Lambert, C. J. Key role of the linker in pyrene-linker-carboxylate surfactants for the efficient aqueous dispersion of multiwalled carbon nanotubes. *RSC Adv.* **2015**, *5*, 95360−95368.
(42) Backes, C.; Hauke, F.; Hirsch, A. The potential of perylene bisimide derivatives for the solubilization of carbon nanotubes and graphene. *Adv. Mater.* **2011**, *23*, 2588−2601.
(43) Fernández-Merino, M. J.; Paredes, J. I.; Villar-Rodil, S.; Guardia, L.; Solís-Fernández, P.; Salinas-Torres, D.; Cazorla-Amorós, D.; Morallón, E.; Martínez-Alonso, A.; Tascón, J. M. D. Investigating the influence of surfactants on the stabilization of aqueous reduced graphene oxide dispersions and the characteristics of their composite films. *Carbon* **2012**, *50*, 3184−3194.
(44) Mohamed, A.; Ardyani, T.; Bakar, S. A.; Brown, P.; Hollamby, M.; Sagisaka, M.; Eastoe, J. Graphene-philic surfactants for nanocomposites in latex technology. *Adv. Colloid Interface Sci.* **2016**, *230*, 54−69.
(45) Jones, D. K.; Kertesz, M.; Gavvalapalli, N. Impact of the Aryl Amphiphile Hydrophobe Size on Controlling the π-Conjugated Microcrystal Growth along the π-Stack Direction. *Cryst. Growth Des.* **2021**, *21*, 2465−2473.
(46) Jones, D. K.; Cheng, C.-H.; Li, Z.; Zhang, X.; Deotare, P. B.; Gavvalapalli, N. Waveguiding properties of perylene microcrystals synthesized by retarding the growth along the π-stack direction. *Chem. Commun.* **2021**, *57*, 3111−3114.

https://doi.org/10.1021/acsomega.1c03126
ACS Omega 2021, 6, 20068−20075

(47) Israelachvili, J. N. *Intermolecular and Surface Forces*, 3rd ed.; Elsevier Science & Technology, 2010.
(48) Ciesielski, A.; Samori, P. Graphene via sonication assisted liquid-phase exfoliation. *Chem. Soc. Rev.* **2014**, *43*, 381−398.

https://doi.org/10.1021/acsomega.1c03126
ACS Omega 2021, 6, 20068−20075